Scanning micro-x-ray diffraction unveils the distribution of oxygen chain nanoscale puddles in $YBa_2Cu_3O_{6.33}$

Gaetano Campi,[1] Alessandro Ricci,[2] Nicola Poccia,[3] Luisa Barba,[4] Gianmichele Arrighetti,[4] Manfred Burghammer,[5] Alessandra Stella Caporale,[6] and Antonio Bianconi[1,6,7]

[1]*Institute of Crystallography, CNR, via Salaria Km 29.300, Monterotondo Roma, 00015, Italy*
[2]*Deutsches Elektronen-Synchrotron DESY, Notkestraße 85, D-22607 Hamburg, Germany*
[3]*MESA + Institute for Nanotechnology, University of Twente, P. O. Box 217, 7500AE Enschede, Netherlands*
[4]*Elettra Sincrotrone Trieste. Strada Statale 14 - km 163, 5, AREA Science Park, 34149 Basovizza, Trieste, Italy*
[5]*European Synchrotron Radiation Facility, B. P. 220, F-38043 Grenoble Cedex, France*
[6]*RICMASS Rome International Center for Materials Science Superstripes, via dei Sabelli 119A, 00185 Roma, Italy*
[7]*Department of Physics, Sapienza University of Rome, 00185 Rome, Italy*

(Received 29 November 2012; revised manuscript received 17 January 2013; published 30 January 2013)

Oxygen chain fragments are known to appear at the insulator-to-superconductor transition in $YBa_2Cu_3O_{6+y}$. However, the self-organization and the size distribution of oxygen chain fragments are not known. Here, we seek to fill this gap, using scanning micro-x-ray diffraction, which is an imaging method based on advances in focusing a synchrotron radiation beam. This approach allows us to probe both real-space and k-space of high-quality $YBa_2Cu_3O_{6.33}$ single crystals with $T_c = 7$ K. We report compelling evidence for nanoscale striped puddles, with Ortho-II structure, made of chain fragments in the basal Cu(1) plane with local oxygen concentration $y \geqslant 0.5$. The size of the Ortho-II puddles spans a range between 2 and 9 nm. The real-space imaging of Ortho-II puddles granular network shows that superconductivity, at a low hole-doping regime, occurs in a network of nanoscale oxygen ordered patches, interspersed with oxygen depleted regions. The manipulation by thermal treatments of the striped Ortho-II puddles has been investigated focusing on the spontaneous symmetry breaking near the order-to-disorder phase transition at $T_0 = 350$ K.

DOI: 10.1103/PhysRevB.87.014517 PACS number(s): 74.70.Xa, 61.05.cf, 64.75.Nx

I. INTRODUCTION

High-temperature superconductivity (HTS) appears in composite materials made of stacks of active superconducting layers intercalated by spacer layers.[1] In $YBa_2Cu_3O_{6+y}$,[2] the active layers are made of an infinite layer cuprate, $Y[Cu(2)O_2]_2$, intercalated with the spacer oxide block made of a defective rocksalt oxide, $[BaO]_2Cu(1)Oi_y$. In the defective spacer oxide block, the oxygen defect ions Oi_y partially fill the empty basal plane sites. Inhomogeneity is a generic feature of HTS because of the electronic phase separation near the charge transfer Mott phase, where metallic stripes,[3] hosting the doped holes with $O(2p^5)Cu(3d^9)$ configuration,[4] coexist with antiferromagnetic domains. Moreover, the lattice diverges from the average structure[5] because of (i) unscreened defects in the spacer layers and (ii) corrugated CuO_2 short-range nanodomains driven by polaronic local lattice distortions[6] and the lattice misfit strain between active and spacer blocks.[7,8] While, in the past years, lattice inhomogeneity was not considered an essential parameter in the search of the mechanism of HTS, recently, the interest on the role of defects for controlling the critical temperature is growing.[9] While disorder usually suppresses the superconducting critical temperature (T_c) in conventional superconductors, an optimum lattice inhomogeneity has been found to enhance the T_c in HTS.[10,11] The tendency toward electronic phase separation in strongly correlated multiband systems with polaronic and Fermi particles near a Mott transition is now well accepted.[12–15] Recently, several theories have been proposed based on the presence in HTS of networks of nanoscale superconducting grains.[16–21]

The nanoscale phase separation related to the self-organization of defects is not a unique feature of cuprates like superoxygenated La_2CuO_{4+y},[22] $La_{2-x}Sr_xCuO_4$,[6,23,24] and $Bi_2Sr_2CaCu_2O_{8+y}$,[25] but it has been found also in $Al_{1-x}Mg_xB_2$,[26] doped iron-chalcogenides,[27–29] and other functional materials like manganites.[30] Thermal treatments control defect organization[31–34] on photo-induced effects,[35] muon-spin resonance (μSR)[36] showed that lattice complexity controls T_c in $YBa_2Cu_3O_{6+y}$. However, direct information concerning lattice inhomogeneity in $YBa_2Cu_3O_{6+y}$[37] is missing because of lack of suitable experimental methods.

In this paper, we used the novel scanning micro-x-ray diffraction (μXRD)[11,22] to unveil the lattice complexity in $YBa_2Cu_3O_{6+y}$. We focused on the size distribution and imaging of the spatial distribution of oxygen Oi chain fragments in the basal plane near the insulator-to-superconductor transition (SIT), and we studied the effect of thermal treatments.[38,39] The satellite superstructure streaks in the XRD pattern of $YBa_2Cu_3O_{6+y}$ probing the metamorphic phase with local oxygen concentration $y = 0.5$ and called Ortho-II by Nakazawa *et al.*,[40] have been observed in the range $0.33 < y < 0.62$.[41–43] We analyzed these superstructures to get the size distribution of the nanoscale Ortho-II puddles and their spatial distribution.

II. MATERIALS AND METHODS

The single crystals of $YBa_2Cu_3O_{6.33}$ were grown using barium zirconate crucibles by the self-flux technique using chemicals of 99.999% purity for CuO and Y_2O_3, and 99.997% for $BaCO_3$.[44,45] The purity of the crystals was found to be better than 99.99 at.% by analysis using inductively coupled plasma mass spectroscopy.

The oxygen content of the crystal was set to 6.33 by annealing in flowing oxygen at 914 °C followed by quenching to room temperature under flowing nitrogen gas. The macroscopic oxygen content inhomogeneity was removed by annealing the crystal at 570 °C in a tiny sealed quartz capsule followed by quenching in an ice-water bath. The crystal was then kept at room temperature to let the short-range oxygen order to develop.[46]

We investigated the sample superstructure due to nanoscale puddles of self-organized oxygen ions filling about 1/3 of the sites on the basal plane.

The structure was investigated with two advanced methods made possible by the use of synchrotron radiation: (i) XRD in transmission mode using a high energy photon beam and (ii) scanning μXRD in reflection.

The source of the 12.4-KeV x rays for scanning μXRD at the ID13 beamline of the *European Synchrotron Radiation Facility* (ESRF) was an electron undulator. The crystal optics include a tapered glass capillary. It produced a 1-μm beam spot at the sample. A charge-coupled device (CCD) area detector recorded the x rays scattered by the sample.[22]

The source of the 20-KeV x-ray beam was the XRD1 beamline of the Elettra Synchrotron in Trieste, Italy. The diffraction patterns as a function of temperature were collected by means of a K-diffractometer with a motorized goniometric xy stage head and a Mar-Research 165-mm CCD camera, 70 mm from the sample. The 20-KeV x-ray beam was selected from the source by a double-crystal Si(111) monochromator.[38]

III. RESULTS AND DISCUSSION

A typical x-ray synchrotron diffraction pattern of the $YBa_2Cu_3O_{6.33}$ in transmission mode, probing the bulk structure, is depicted in Fig. 1(a). The lattice parameters are $a = 3.851(4)$ Å, $b = 3.856(4)$ Å, and $c = 11.78(5)$ Å. The Cu-O bond distance is 192.8 pm, showing a 2% compression relative with the Cu-O equilibrium distance of 197 pm.[47]

Therefore, this sample is near the optimum misfit strain[7,8] and the SIT transition. Visual inspection of the 2D diffraction pattern in Fig. 1(a) shows immediately the satellite reflections $q_{ortho\text{-}II}$ ($h \pm 0.5$,k,l) between the principal reflections associated with ordered oxygen chains fragments forming nanoscale Ortho-II puddles.

These $q_{ortho\text{-}II}$ satellites have a needle shape clearly pointing in both horizontal and vertical directions. The equal intensity of vertical and horizontal streaks indicates a phase with an equal number of horizontal and vertical puddles. A pictorial view of the phase separation derived from these data is shown in Fig. 1(b). The oxygen-rich Oi chain fragments form nanoscale Ortho-II puddles coexisting with oxygen-poor domains with disordered Oi_y.

The point-to-point spatial variation of the size of the Ortho-II puddles was measured by scanning μXRD in reflection using the 12.4-KeV x rays focused on a micron-sized spot and probing a thickness of about 1 μm.[22] The (0.5,0,3) superstructure satellite reflection was measured at each point (x,y) of the sample reached by the x-y translator with micron resolution. The integrated intensity of the superstructure peaks and their position in different spots of the crystal were quite homogenous ($q_{ortho\text{-}II} = 0.5$ with a standard deviation of 0.001). This indicated that the nanoscale oxygen puddles had the Ortho-II periodicity and confirmed the high quality of the crystal. On the contrary, the full width half-maximum (FWHM) of the peaks showed significant variations from point

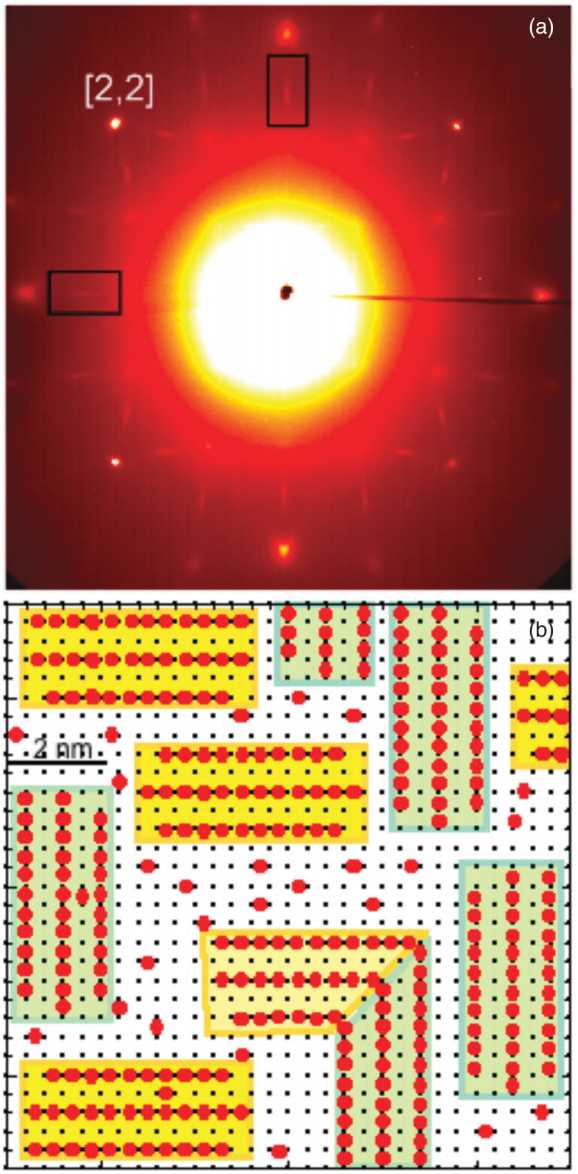

FIG. 1. (Color online) (a) The diffraction pattern in the (h,k) plane of $YBa_2Cu_3O_{6.33}$ ($T_c = 7$ K) measured in transmission mode on a 100-μm-thick sample with c axis oriented in the x-ray beam direction. Here, 20-KeV photon energy and 100-μm x-ray beam size have been used. The diffuse streaks $q_{ortho\text{-}II}$ at ($h \pm 0.5$,0) are superstructure satellites due to nanoscale puddles with Ortho-II structure made by Oi ordering after annealing at 300 K. The equal intensity of horizontal and vertical streaks highlighted with the black rectangles indicate a phase made of the Ortho-II puddles where the a axis is oriented both in the vertical and horizontal direction. (b) Pictorial view of the basal Cu-Oi_y plane of $YBa_2Cu_3O_{6+y}$. The small black dots are the Cu(1) sites, and the large red dots are the oxygen defect ions Oi_y. Horizontal and vertical oxygen-rich metamorphic phase ($y = 0.5$) called Ortho-II by Nakazawa *et al.*[40] The Ortho-II puddles are intercalated by disordered oxygen-poor ($y < 0.33$) domains. The black bar indicates 2-nm length scale.

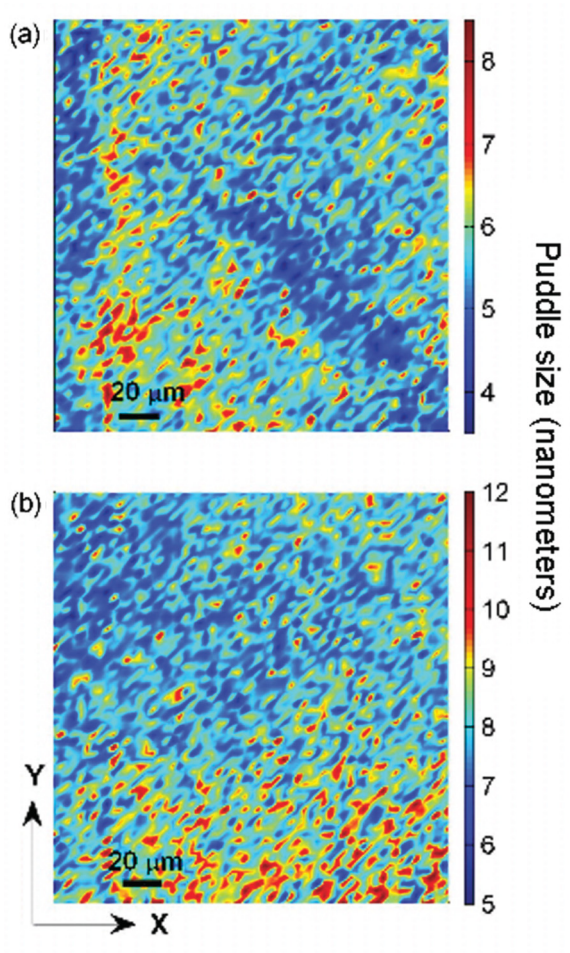

FIG. 2. (Color online) Scanning micro-x-ray diffraction of a single crystal $YBa_2Cu_3O_{6.33}$ using a 12-KeV energy and probing 1-μm thickness of the crystal surface. The puddle size (color) of the Ortho-II puddles is plotted as a function of the illuminated spot position xy in the sample surface, where x and y direction in the image correspond to the a and b crystallographic axis of the sample. The size of the Ortho-II oxygen chain puddles, averaged over 1-μm illuminated spots, changes from site to site. It ranges from 3 (dark blue) to 12 nm (red) in the (a) a-axis direction and in the (b) c-axis direction. The white bar indicates 20-μm length scale on the sample surface.

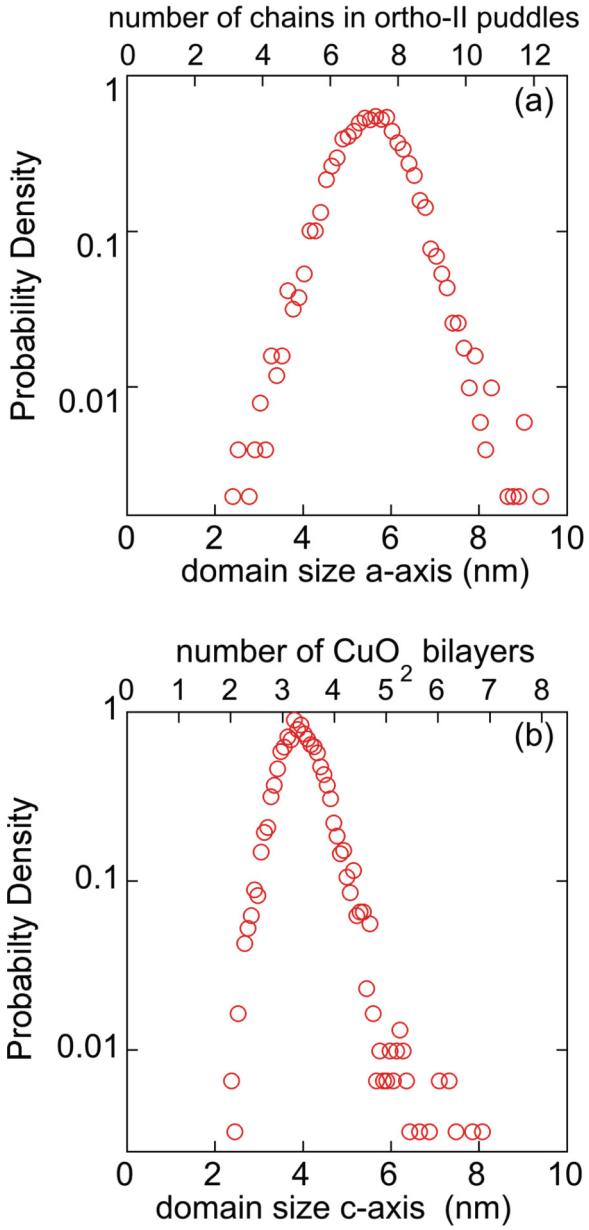

FIG. 3. (Color online) Statistical distribution of the size of the Ortho-II puddles from data shown in Fig. 2. (a) and (b) The probability distribution function of spots in the crystal where the Ortho-II puddles have the same size in the a-axis [c axis in (b)] direction. The puddle size in nanometers is determined from the FWHM of superstructure diffraction $q_{ortho\text{-}II}$ satellite reflections in the $a*$ [$c*$ in (b)] direction. The measured size of the Ortho-II puddles shows that the number of chains is bigger than the number of CuO_2 bilayers in each puddle. This is related with a larger mobility of oxygen defects in the basal plane.

to point: Indeed, the domain size of the Ortho-II puddles, derived from the measured FWHM via standard methods of diffraction[43] ranged between 3 and 9 nm. Upon inspection of the real-space mapping of the nanoscale Ortho-II puddles sizes shown in Fig. 2, the heterogeneous granular structure appeared quite clearly. The puddle sizes were derived from the inverse of the superstructure satellites FWHM in the k-space along the $a*$ (panel a), $c*$ (panel b) directions. More specifically, the FWHM of the diffraction profiles in the h direction probed the size of the Ortho-II puddles transverse to the chains direction, i.e. provided the number of chain fragments in a puddle.

At the same time, the FWHM in the $c*$ direction of the reciprocal lattice probed the chain fragment length along the c axis direction. The statistical analysis of the Ortho-II puddles sizes is shown in Fig. 3: The probability distributions of the length of the chain fragments [Fig. 3(a)] and their size along the c axis [Fig. 3(b)] show that the Ortho-II puddles are made of 2.5 to 12 oxygen chains oriented along the a axis [Fig. 3(a)] in domains with an average size of 4 nm and a standard deviation of 0.6 nm along the c crystallographic direction [Fig. 3(b)]. We observed clear irregularities and deviations from normal behavior in the distribution tails. In order to quantify these deviations, we calculated the distribution skewness sk giving

$sk_a = 0.3$ and $sk_c = 0.9$ for the Ortho-II domain size along the a and c directions, respectively. Their positive values indicated a larger weight of the right tails in both distributions, while the fact that sk_c is substantially larger than sk_a confirmed accentuated disorder in the out-of-plane direction.

The size distribution was averaged over a 1-μm area that was much smaller than in many other x-ray or neutron diffraction experiments reported, but it was much larger than the size of the puddles. Therefore, additional insight could be gained by carrying out investigations with smaller nanometer beams.

Having determined the spatial imaging and distributions of the Ortho-II puddles, we moved to the effects of thermal treatments. The diffraction patterns as a function of temperature were collected at the XRD1 beamline of the Elettra Synchrotron. The temperature of the crystals was increased from 270 to 400 K using a cryocooler (700 series Oxford Cryosystems). The heating cycle was carried out at quite a slow rate (0.2 K/minute). For the temperature cycles, the sample was sealed in an oxygen-filled ampoule, and it was kept only a few minutes above 350 K in the thermal cycle without any loss of oxygen out of the sample surface and no change in the overall stoichiometry, as shown by the fact that the sample went back to the same phase as the as-grown crystal after a month. Figure 4 shows the 3D temperature evolution of the (2.5,0,0) Ortho-II satellite profile along h and k, respectively.

Although the order-to-disorder phase transition was at $T_0 = 350 \pm 5$ K, we can appreciate the presence of smaller nanoscale Ortho-II puddles above T_0, up to 400 K, in agreement with previous work.[25,26] After the heating, we completed our thermal cycle with a cooling ramp performed at the same heating rate. The variations of the intensity and of the FWHM of the Ortho-II superstructure diffraction profiles during the whole cycle are plotted in Fig. 5. Here, the FWHM in the k direction of the reciprocal lattice probes the chain fragment length along the b axis direction. We observed a relevant hysteresis (Fig. 5), demonstrating that once the Ortho-II nanopuddles of oxygen chains are formed, they cannot be reformed in a reversible way, with the same size, in the timescale of the experiment.

As shown in Fig. 1, the Ortho-II puddles were equally oriented in the horizontal and vertical direction of the sample with $y = 0.33$, giving diffraction streaks broad and diffuse in the h direction and narrow in the k direction. The broad and diffuse streaks were observed both in the vertical and horizontal direction, indicating vertical and horizontal puddles. In the as-grown sample, we observed the same diffraction intensity and the same width of horizontal and vertical streaks, showing that the average size of Ortho-II puddles is the same for vertical and horizontal puddles. Increasing the temperature above the order-to-disorder transition, the size of the Ortho-II puddles decreased, as shown in Fig. 5(d). In the heating cycle, a large difference between the size of vertical and horizontal Ortho-II puddles appeared in the temperature range of 350 K $< T <$ 380 K above the order-to-disorder phase transition temperature ($T_0 = 350$ K). A smaller variation in the 320 K $< T <$ 350 K temperature range, below the phase transition temperature, was observed [Fig. 5(d)]. This large anisotropy due to preferential ordering emerged in the fluctuation regime above the order-to-disorder critical temperature $T_0 = 350$ K. This phenomenon provides evidence for spontaneous symmetry breaking in the fluctuation regime near the order-to-disorder phase transition temperature.

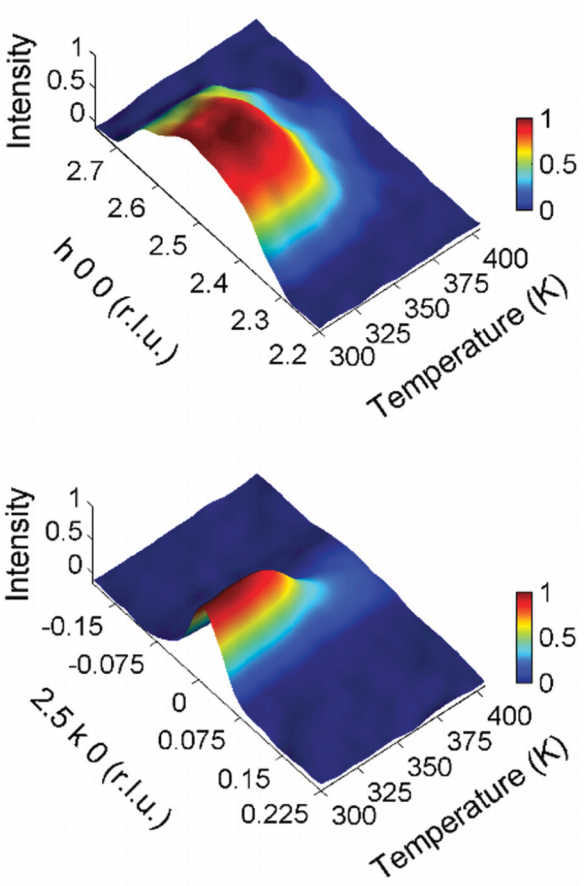

FIG. 4. (Color online) Temperature evolution of the $q_{ortho\text{-}II}$ satellite reflection profiles along h (upper panel) and k (lower panel). The bright (red online) and dark (blue online) color corresponds, respectively, to the higher and lower intensities of the satellite diffraction spots. Variation of the average structure of Ortho-II puddles in the (h,k) plane of $YBa_2Cu_3O_{6.33}$ measured in transmission mode of a 100-μm-thick sample using an x-ray beam of 20-KeV photon energy and 100-μm size.

IV. DISCUSSION

We investigated the variation of the Ortho-II puddles size from point to point in a very good crystal using a novel mixed k-space and r-space probe of bulk heterogeneity combining high wave number resolution with micrometer-scale spatial resolution.

The scanning μXRD is similar to transmission electron microscopy (TEM), but without the complication of electron beam damage. In fact, the electron beam heating of the thin crystals can change the mobile oxygen content y and generate transient nonequilibrium surface structures that mask intrinsic bulk effects. Therefore, information of finite size ordering properties as well as temperature-dependent properties is not achievable by TEM.

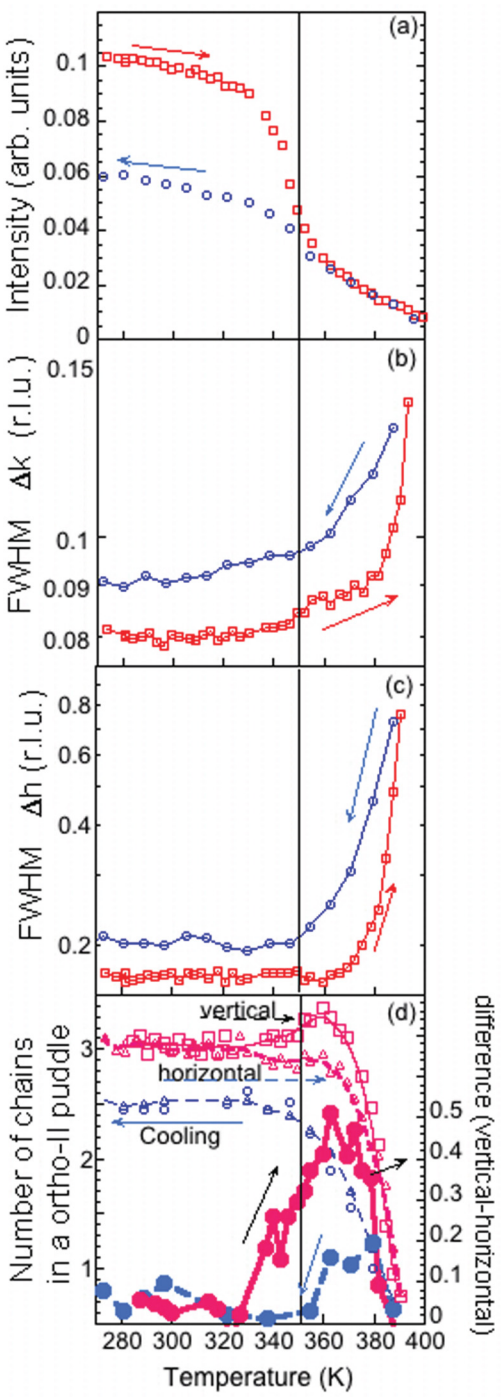

FIG. 5. (Color online) Temperature evolution of the $q_{ortho\text{-}II}$ superstructure in the heating cycle followed by the cooling cycle. The average normalized intensity as a function of temperature is shown in (a). The squares (red online) and circles (blue online) represent the data collected during the heating and cooling thermal cycles, respectively. The average FWHM along the $b*$ and $a*$ directions are plotted in (b) and (c), respectively. (d) The variation of the size of the Ortho-II puddles oriented in the vertical (open squares red online) and horizontal (open triangles) direction in the sample, during the warming cycle. The difference between the size of vertical and horizontal Ortho-II puddles indicated by large filled (red online) dots (filled dots, blue online) in the heating (cooling) cycle shows a large value in the range 350 K $< T <$ 380 K due to the spontaneous symmetry breaking in the fluctuation regime above 350 K.

The application of scanning μXRD for imaging the nanoscale phase separation in $YBa_2Cu_3O_{6.33}$ showed the presence of a phase of nanoscale Ortho-II puddles embedded in an insulating oxygen-poor background in a sample very close to the superconductor-insulator phase transition. The network of the Ortho-II puddles was made of different puddles ranging between 3 and 12 oxygen chains.

The scanning μXRD and the temperature treatments show that the local structure in $YBa_2Cu_3O_{6+y}$ deviates from the ideal one. We saw a relevant structure dependence with temperature in agreement with previous high-resolution XRD data, where temperature treatments modify the density and elongation of the Cu-O chains.[43–46] The formation of nanoscale ordered grains in $YBa_2Cu_3O_{6+y}$ with Ortho-II lattice in the basal plane is highly relevant for the electronic structure of the system and for models of superconductor-to-insulator transition.[19,20] The oxygen chain puddles had the Ortho-II lattice superstructure, like the $YBa_2Cu_3O_{6.5}$, which showed band folding and Fermi surface reconstruction measured by photoemission and quantum oscillations experiments.[48,49] The granular structure of Ortho-II puddles favored the 7 K superconductivity; in fact, in the rapidly quenched sample from $T > 450$ K, where the Ortho-II puddles were not formed, the critical temperature drops to zero.

The nanoscopic phase separation of the oxygen puddles described here using μXRD could explain why zero and transverse field μSR experiments have shown the coexistence of antiferromagnetic short-range magnetism with superconductivity in $YBa_2Cu_3O_{6+y}$ with $6.37 < y < 6.39$.[50] In fact, since the average oxygen concentration is 6.33 and the local oxygen concentration in the Ortho-II puddles is 6.5, we deduce that, in the intercalated spatial portions, the oxygen concentration y has to be smaller than 6.33. In this way, the oxygen puddles are expected to cover 66% of the space; in contrast with the not percolating nanoscopic magnetic portions. This explains why neutron scattering experiments do not find a static antiferromagnetism.[50] On the other hand, both neutron scattering and μSR experiments agree with the presence of two energy scales and short-ranged correlations. A similar granular disorder has been found also in single crystals of La_2CuO_{4+y}[11,22,38,39] and of $Bi_2Sr_2CaCu_2O_{8+y}$[25] using scanning μXRD.

Our noninvasive technique μXRD probes portions of the single crystals of 1 μm size, much smaller than those seen by neutron diffraction and previous x-ray diffraction,[26] and therefore allows us to measure the formation of nanocrystalline puddles with very good spatial resolution.

V. CONCLUSION

We used scanning μXRD to probe the microscopic spatial inhomogeneity in $YBa_2Cu_3O_{6.33}$, which cannot be visualized through standard averaged XRD. The spatial resolution of 1 μm used in our measurements allowed us to clearly visualize the granular nanoscopic phase separation due to the formation of the network of Ortho-II puddles made of oxygen ordered chains. We measured the size of the nanoscale oxygen ordered puddles in $YBa_2Cu_3O_{6+y}$ near the superconductor-to-insulator phase transition, showing the breakdown of the standard model for cuprates, assuming a homogenous distribution of dopants.

On the contrary, we clearly unveiled the granular structure of superconducting grains of 5–10-nm size of $YBa_2Cu_3O_{6.5}$ embedded in an insulating background $YBa_2Cu_3O_6$, supporting the theories of high-temperature superconductors made of complex networks of percolating superconducting grains.[19,20]

ACKNOWLEDGMENTS

We thank Ruixing Liang, D. A. Bonn, and Walter N. Hardy of the Department of Physics of the University of British Columbia for providing us with the crystals and for helpful discussions.

[1] A. Bianconi, Solid State Commun. **89**, 933 (1994).

[2] M. K. Wu, J. R. Ashburn, C. J. Torng, P. H. Hor, R. L. Meng, L. Gao, Z. J. Huang, Y. Q. Wang, and C. W. Chu, Phys. Rev. Lett. **58**, 908 (1987).

[3] J. Zaanen and O. Gunnarsson, Phys. Rev. B **40**, 7391 (1989).

[4] A. Bianconi, A. Congiu-Castellano, M. De Santis, P. Rudolf, P. Lagarde, A. M. Flank, and A. Marcelli, Solid State Commun. **63**, 1009 (1987).

[5] T. Egami and S. J. L. Billinge, *Underneath the Bragg Peaks* (Pergamon, Oxford, 2003), Vol. 16.

[6] A. Bianconi, N. L. Saini, A. Lanzara, M. Missori, T. Rossetti, H. Oyanagi, H. Yamaguchi, K. Oka, and T. Ito, Phys. Rev. Lett. **76**, 3412 (1996).

[7] A. Bianconi, N. L. Saini, S. Agrestini, D. Di Castro, and G. Bianconi, Int. J. Mod. Phys. B **14**, 3342 (2000); A. Bianconi, D. Di Castro, G. Bianconi, A. Pifferi, N. L. Saini, F. C. Chou, D. C. Johnston, and M. Colapietro, Physica C **341**, 1719 (2000).

[8] A. Bianconi, S. Agrestini, G. Bianconi, D. Di Castro, and N. L. Saini, J. Alloys Compd. **317–318**, 537 (2001).

[9] P. Littlewood, Nat. Mater. **10**, 726 (2011).

[10] T. H. Geballe and M. Marezio, Physica C **469**, 680 (2009).

[11] N. Poccia, A. Ricci, G. Campi, M. Fratini, A. Puri, D. D. D. Gioacchino, A. Marcelli, M. Reynolds, M. Burghammer, N. L. L. Saini, and A. Bianconi, Proc. Nat. Acad. Sci. USA **109**, 15685 (2012).

[12] L. P. Gor'kov and G. B. Teitel'baum, Phys. Rev. B **82**, 020510 (2010).

[13] K. I. Kugel, A. L. Rakhmanov, A. O. Sboychakov, N. Poccia, and A. Bianconi, Phys. Rev. B **78**, 165124 (2008).

[14] D. Innocenti, A. Ricci, N. Poccia, G. Campi, M. Fratini, and A. Bianconi, J. of Superconductivity and Novel Magn. **22**, 529 (2009).

[15] A. Bianconi and M. Missori, Solid State Commun. **91**, 287 (1994).

[16] A. Perali, A. Bianconi, A. Lanzara, and N. L. Saini, Solid State Commun. **100**, 181 (1996).

[17] V. Kresin, Y. Ovchinnikov, and S. Wolf, Phys. Rep. **431**, 231 (2006).

[18] E. V. L. de Mello, Europhys. Lett. **98**, 57008 (2012).

[19] G. Bianconi, Phys. Rev. E **85**, 061113 (2012).

[20] G. Bianconi, J. Stat. Mech.: Theory and Experiment (2012) P07021.

[21] J. Zaanen, Nature **466**, 825 (2010).

[22] M. Fratini, N. Poccia, A. Ricci, G. Campi, M. Burghammer, G. Aeppli, and A. Bianconi, Nature **466**, 841 (2010).

[23] N. L. Saini, H. Oyanagi, T. Ito, V. Scagnoli, M. Filippi, S. Agrestini, G. Campi, K. Oka, and A. Bianconi, Eur. Phys. J. B **36**, 75 (2003).

[24] E. S. Božin, G. H. Kwei, H. Takagi, and S. J. L. Billinge, Phys. Rev. Lett. **84**, 5856 (2000).

[25] N. Poccia, G. Campi, M. Fratini, A. Ricci, N. L. Saini, and A. Bianconi, Phys. Rev. B **84**, 100504 (2011).

[26] G. Campi, E. Cappelluti, Th. Proffen, X. Qiu, E. S. Bozin, S. J. L. Billinge, S. Agrestini, N. L. Saini, and A. Bianconi, Eur. Phys. J. B **52**, 15 (2006).

[27] V. Ksenofontov, G. Wortmann, S. A. Medvedev, V. Tsurkan, J. Deisenhofer, A. Loidl, and C. Felser, Phys. Rev. B **84**, 180508 (2011).

[28] A. Charnukha, J. Deisenhofer, D. Pröpper, M. Schmidt, Z. Wang, Y. Goncharov, A. N. Yaresko, V. Tsurkan, B. Keimer, A. Loidl, and A. V. Boris, Phys. Rev. B **85**, 100504 (2012).

[29] A. Ricci, N. Poccia, G. Campi, B. Joseph, G. Arrighetti, L. Barba, M. Reynolds, M. Burghammer, H. Takeya, Y. Mizuguchi, Y. Takano, M. Colapietro, N. L. Saini, and A. Bianconi, Phys. Rev. B **84**, 060511 (2011); A. Ricci, N. Poccia, B. Joseph, G. Arrighetti, L. Barba, J. Plaisier, G. Campi, Y. Mizuguchi, H. Takeya, Y. Takano *et al.*, Supercond. Sci. Technol. **24**, 082002 (2011).

[30] E. Dagotto, *Nanoscale Phase Separation and Colossal Magnetoresistance: The Physics of Manganites and Related Compounds* (Springer, New York, 2003), http://www.springer.com/materials/book/978-3-540-43245-6.

[31] J. D. Jorgensen, S. Pei, P. Lightfoor, H. Shi, A. P. Paulikas, and B. W. Veal, Physica C **167**, 571 (1990).

[32] B. W. Veal, A. P. Paulikas, H. You, H. Shi, Y. Fang, and J. W. Downey, Phys. Rev. B **42**, 6305 (1990).

[33] G. Ceder, R. McCormack, and D. de Fontaine, Phys. Rev. B **44**, 2377 (1991).

[34] H. Friis Poulsen, N. Hessel Andersen, J. Vrtting Andersen, H. Bohrt, and O. G. Mouritsen, Nature **349**, 594 (1991).

[35] G. Yu, C. H. Lee, A. J. Heeger, N. Herron, E. M. McCarron, L. Cong, G. C. Spalding, C. A. Nordman, and A. M. Goldman, Phys. Rev. B **45**, 4964 (1992).

[36] S. Sanna, G. Allodi, G. Concas, A. D. Hillier, and R. De Renzi, Phys. Rev. Lett. **93**, 207001 (2004).

[37] C. L. Johnson, J. K. Bording, and Y. Zhu, Phys. Rev. B **78**, 014517 (2008).

[38] N. Poccia, M. Fratini, A. Ricci, G. Campi, L. Barba, A. Vittorini-Orgeas, G. Bianconi, G. Aeppli, and A. Bianconi, Nat. Mater. **10**, 733 (2011).

[39] N. Poccia, A. Bianconi, G. Campi, M. Fratini, and A. Ricci, Supercond. Sci. Technol. **25**, 124004 (2012).

[40] Y. Nakazawa, M. Ishikawa, T. Takabatake, K. I. Koga, and K. Terakura, Jpn. J. Appl. Phys. **26**, L796 (1987).

[41] R. Liang, D. A. Bonn, and W. N. Hardy, Physica C **336**, 57 (2000).

[42] J. Strempfer, I. Zegkinoglou, U. Rütt, M. V. Zimmermann, C. Bernhard, C. T. Lin, Th. Wolf, and B. Keimer, Phys. Rev. Lett. **93**, 157007 (2004).

[43] M. von Zimmermann, J. R. Schneider, T. Frello, N. H. Andersen, J. Madsen, M. Käll, H. F. Poulsen, R. Liang, P. Dosanjh, and W. N. Hardy, Phys. Rev. B **68**, 104515 (2003).

[44] Ruixing Liang, D. A. Bonn, and W. N. Hardy, Philos. Mag. **92**, 2356 (2012).

[45]Ruixing Liang, D. A. Bonn, and W. N. Hardy, Physica C **304**, 105 (1998).

[46]R. Liang, D. A. Bonn, W. N. Hardy, J. C. Wynn, K. A. Moler, L. Lu, S. Larochelle, L. Zhou, M. Greven, L. Lurio, and S. G. J. Mochrie, Physica C **383**, 1 (2002).

[47]J. Garcia, A. Bianconi, M. Benfatto, and C. R. Natoli, J. Phys. Colloques **47**, C8-49 (1986).

[48]Y. Sassa, M. Radović, M. Maansson, E. Razzoli, X. Y. Cui, S. Pailhès, S. Guerrero, M. Shi, P. R. Willmott, F. M. Granozio, J. Mesot, M. R. Norman, and L. Patthey, Phys. Rev. B **83**, 140511 (2011).

[49]D. Fournier, G. Levy, Y. Pennec, J. L. McChesney, A. Bostwick, E. Rotenberg, R. Liang, W. N. Hardy, D. A. Bonn, I. S. Elfimov, and A. Damascelli, Nat. Phys. **6**, 905 (2010).

[50]C. Stock, W. J. L. Buyers, Z. Yamani, C. L. Broholm, J. H. Chung, Z. Tun, R. Liang, D. Bonn, W. N. Hardy, and R. J. Birgeneau, Phys. Rev. B **73**, 100504 (2006).